The Journal of Immunology

IFN-γ–Dependent Reduction of Erythrocyte Life Span Leads to Anemia during Mycobacterial Infection

Ana Cordeiro Gomes, Ana C. Moreira, Tânia Silva, João V. Neves, Gonçalo Mesquita, Agostinho A. Almeida, Palmira Barreira-Silva, Rui Fernandes, Mariana Resende, Rui Appelberg, Pedro N. S. Rodrigues and Maria Salomé Gomes

J Immunol 2019; 203:2485-2496; Prepublished online 27 September 2019;
doi: 10.4049/jimmunol.1900382
http://www.jimmunol.org/content/203/9/2485

The Journal of Immunology is published twice each month by
The American Association of Immunologists, Inc.,
1451 Rockville Pike, Suite 650, Rockville, MD 20852

Print ISSN: 0022-1767 Online ISSN: 1550-6606.

IFN-γ–Dependent Reduction of Erythrocyte Life Span Leads to Anemia during Mycobacterial Infection

Ana Cordeiro Gomes,[*,†,‡] Ana C. Moreira,[*,†,‡,1] Tânia Silva,[*,†,1] João V. Neves,[*,†] Gonçalo Mesquita,[*,†] Agostinho A. Almeida,[§] Palmira Barreira-Silva,[¶,‖] Rui Fernandes,[*,†] Mariana Resende,[*,†] Rui Appelberg,[*,†,‡] Pedro N. S. Rodrigues,[*,†,‡] and Maria Salomé Gomes[*,†,‡]

Anemia is a frequent and challenging complication of mycobacterial infections. We used a model of disseminated *Mycobacterium avium* infection in mice to investigate the mechanisms of mycobacteria-induced anemia. We found increased formation of RBC in the bone marrow and spleen of infected mice. Infection induced reticulocytosis and the premature egress of immature progenitors to the systemic circulation in an IFN-γ (IFNG)–dependent way. The newly formed RBC had reduced CD47 surface expression and a reduced life span and were phagocytosed in the liver of infected mice, increasing iron recycling in this organ. The increased engulfment and degradation of RBC was independent of IFNG sensing by macrophages. Together, our findings demonstrate that mycobacterial infection alters the formation of erythrocytes, leading to their accelerated removal from circulation and hemolytic anemia. This comprehensive elucidation of the mechanisms underlying mycobacteria-induced anemia has important implications for its efficient clinical management. ***The Journal of Immunology*****, 2019, 203: 2485–2496.**

Mycobacteria are a large and diverse group of bacteria, enclosing some of the deadliest human pathogens: *Mycobacterium tuberculosis*, which causes tuberculosis (TB) (1), and *Mycobacterium leprae*, which is responsible for leprosy. Additionally, the incidence of infections by nontuberculous mycobacteria (species other than *M. tuberculosis* and *M. leprae*) is increasing, and these infections tend to be long-lasting and difficult to treat (2, 3). Infections by mycobacteria frequently lead to the development of anemia, which correlates with an increased risk of death during TB (4–7). Disseminated *Mycobacterium avium* disease is particularly common in severely immunocompromised patients. The disease may occur following pulmonary exposure, but most infections develop after ingestion of the bacteria, followed by replication in localized lymph nodes and then by systemic spread. Clinical manifestations of disease are usually not observed until the normal function of an organ is impaired.

The mechanisms of anemia development during mycobacterial infections are not fully understood. Whether mycobacteria-induced anemia is due to iron restriction in response to infection or to a block in RBC formation is still a matter of debate. We have previously used the mouse model of *Mycobacterium avium* infection as a model of mycobacteria-induced anemia (8).

As with many other pathogens, the outcome of *M. avium* infection depends on iron availability, with the host's iron overload causing increased susceptibility to infection and iron deprivation contributing to inhibition of mycobacterial growth (9–11). It is known that nutritional immunity and, in particular, iron deprivation are important ways by which the host may control the pathogen's growth. In this context, the small liver-derived peptide hepcidin is considered a key player. During inflammatory response, macrophages produce IL-6, which induces hepcidin production by hepatocytes. Hepcidin in turn will block cellular iron release through ferroportin and consequently will cause hypoferremia: a decrease in total serum iron levels and in the iron saturation level of the main serum iron transporter transferrin. This hypoferremia is thought to cause a deficiency in iron delivery

*Instituto de Investigação e Inovação em Saúde, Universidade do Porto, 4200-1835 Porto, Portugal; †Instituto de Biologia Molecular e Celular, Universidade do Porto, 4200-1835 Porto, Portugal; ‡Instituto de Ciências Biomédicas de Abel Salazar, Universidade do Porto, 4050-313 Porto, Portugal; §Faculdade de Farmácia, Universidade do Porto, 4200-1835 Porto, Portugal; ¶Life and Health Sciences Research Institute, School of Medicine, Universidade do Minho, 4710-057 Braga, Portugal; and ‖Life and Health Sciences Research Institute/3B's Research Group, PT Government Associate Laboratory, 4710-057 Braga/Guimarães, Portugal

[1]A.C.M. and T.S. contributed equally to this work.

ORCIDs: 0000-0001-5305-8538 (A.C.G.); 0000-0003-4049-4781 (A.C.M.); 0000-0002-6087-1487 (T.S.); 0000-0002-2205-2325 (G.M.); 0000-0002-1297-3198 (A.A.A.); 0000-0002-8070-1856 (P.B.-S.); 0000-0002-9535-368X (R.F.); 0000-0003-4835-3035 (M.R.); 0000-0002-9447-0665 (R.A.); 0000-0001-7657-2118 (M.S.G.).

Received for publication April 3, 2019. Accepted for publication September 4, 2019.

This work was supported by Fundo Europeu de Desenvolvimento Regional (FEDER) funds through the COMPETE 2020–Operacional Programme for Competitiveness and Internationalisation, Portugal 2020, and by Portuguese funds through Fundação para a Ciência e a Tecnologia (FCT)/Ministério da Ciência, Tecnologia e Ensino Superior in the framework of Project PTDC/IMI-MIC/1683/2014 (POCI-01-0145-FEDER-016590). This work also results from Project Norte-01-0145-FEDER-000012, a structured program on bioengineered therapies for infectious diseases and tissue regeneration, supported by Norte Portugal Regional Operational Programme (NORTE 2020), under the PORTUGAL 2020 Partnership Agreement, through FEDER. A.C.M. received Fellowship SFRH/BPD/101405/2014 from the FCT.

A.C.G. conceptualized, designed, and performed experiments and wrote the paper. A.C.M., T.S., J.V.N., G.M., R.F., A.A.A., and P.B.-S. performed experiments and revised the paper. M.R. and R.A. provided mice and reagents and revised the manuscript. P.N.S.R. was involved in fundraising, data discussion, and paper revision. M.S.G. funded, conceptualized, and supervised studies and wrote the paper.

Address correspondence and reprint requests to Prof. Maria Salomé Gomes, Universidade do Porto, IBMC-Instituto de Biologia Molecular e Celular, Rua Alfredo Allen 208, 4200-1835 Porto, Portugal. E-mail address: sgomes@ibmc.up.pt

The online version of this article contains supplemental material.

Abbreviations used in this article: BM, bone marrow; %BrdU$^+$, percentage of cells incorporating BrdU; HSC, hematopoietic stem cell; i3S, Instituto de Investigação e Inovação em Saúde; IFNG, IFN-γ; MEP, megakaryocyte and erythroid progenitor; MFI, mean fluorescence intensity; MPP, multipotent progenitor; p.i., postinfection; Pro-E, proerythroblast; RT, room temperature; TB, tuberculosis; TEM, transmission electron microscopy; WT, wild-type.

to the bone marrow (BM) and, consequently, a decrease in erythrocyte production (12, 13). Previous studies in our group have shown that infection by *M. avium* in mice leads to anemia but does not involve the induction of hepcidin (8). *M. avium* has other impacts on the host's iron metabolism, such as the upregulation of the iron storage protein H ferritin (14) and proteins involved in heme catabolism and iron recycling, such as heme oxygenase 1 (HOMX1) (15). However, it is not clear whether these alterations in iron metabolism are related to the development of anemia.

Infection by *M. avium* causes IFN-γ (IFNG) production (16) that is not only sensed by myeloid cells but also by hematopoietic stem cells (HSC), causing overproliferation of the latter cell population (17). Furthermore, continuous inoculation with *M. avium* skews the hematopoietic development toward myelopoiesis, followed by the exhaustion of the HSC pool and subsequent development of pancytopenia (18). However, pancytopenia arises only in a small percentage of the individuals infected with mycobacteria, whereas anemia is much more common in these patients. Hence, it is possible that different mechanisms underlie anemia and other hematopoietic alterations.

Erythropoiesis involves highly controlled sequential stages of differentiation from HSC to reticulocytes (19). This process usually occurs in BM, but during inflammatory states, erythropoiesis may occur in the spleen (20). From HSC to the megakaryocyte and erythroid progenitor (MEP) stage, erythropoiesis occurs in the hematopoietic niche (21). Then, MEP differentiate into proerythroblasts (Pro-E), which in turn originate erythroblasts (22). Erythroblasts are found surrounding macrophages in erythroblastic islands (23) that support the proliferation, differentiation, and enucleation of erythroblasts (24). Reticulocytes egress from BM to the circulation where, within a week, they differentiate into mature RBC (19). Under homeostatic conditions, circulating erythrocytes are removed from circulation through erythrophagocytosis in the spleen. However, in stress conditions, the liver becomes the major site of RBC degradation (25).

In this study, we addressed how anemia established during mycobacterial infection, using a model of systemic chronic infection by *M. avium*. We found that anemia establishment correlates with a decreased life span of erythrocytes in circulation. We found that besides the overproliferation of HSC and multipotent progenitors, the commitment to the erythroid lineage was not affected. However, erythroid development was slightly faster at the later stages of erythroblast, with reticulocytosis and the premature egress of developing erythrocytes. During infection, the newly formed erythrocytes were smaller, had a lower amount of hemoglobin, and expressed a lower level of CD47. Therefore, we show that the mechanisms of mycobacteria-induced anemia include the reduced life span of erythrocytes, which are increasingly prone to early removal from the circulation.

Materials and Methods

Bacteria

Mycobacterium avium 25291 SmT (obtained from the American Type Culture Collection, Manassas, VA) was grown at 37˚C in Middlebrook 7H9 broth (BD Difco), supplemented with 0.05% of Tween 80 (Sigma-Aldrich, St. Louis, MO) and 10% Albumin-Dextrose-Catalase. Mycobacteria were collected during the exponential growth phase, centrifuged, washed twice with saline containing 0.04% Tween 80, resuspended in the same solution, and briefly sonicated at low power to disrupt bacteria clumps. Aliquots were prepared and stored at −80˚C until needed. Just before use, an aliquot was thawed and diluted to the appropriate concentration.

Mice

C57BL/6J, *Ifng*$^{-/-}$, and MIIG (26) mice were bred and housed under specific pathogen-free conditions at the Instituto de Investigação e Inovação em Saúde (i3S) animal facility. Mice were kept inside individually ventilated cages with HEPA filters and fed with sterilized food and water ad libitum.

Ethics statement

All experimental animal procedures described in this work were approved by the local animal ethics committee of the Instituto de Biologia Molecular e Celular/i3S and licensed by the Portuguese Authority General Directory of Agriculture and Veterinary on July 6th, 2016 (reference no. 0421/000/000/2016). All animals were handled in strict accordance with good animal practice as defined by national authorities General Directory of Agriculture and Veterinary (Decreto-Lei 113/2013, August 7th) and European Directive (2010/63/EU).

In vivo infection

Eight- to ten-week-old mice were infected with 1 million CFU of *M. avium* 25291 SmT i.v. into one of the lateral tail veins. Control groups were injected with the same volume of saline solution by the same route. At 4 or 8 wk postinfection (p.i.), mice were anesthetized using an isoflurane chamber. Blood was collected by retro-orbital puncture under anesthesia. Organs such as the liver and spleen were collected aseptically and weighted. Long bones were also collected.

RBC turnover assay

One milligram of EZ-Link Sulfo-NHS-LC-Biotin (Thermo Fisher Scientific) in a saline solution was administered i.v. in the lateral tail vein to each mouse. Two hours later, blood was collected by retro-orbital bleeding, and the animals were euthanized to enumerate the percentage of biotinylated RBC at timepoint 0. Fourteen days later, the remaining mice were sacrificed, and blood was collected to determine the percentage of remaining biotinylated RBC as readout of RCB turnover.

RBC transfer

Blood from 8-wk-infected and noninfected mice was collected to EDTA-coated tubes (Vacuette; Becton Dickinson) and centrifuged at 500 × *g* for 5 min. RBC were then labeled with CFSE (noninfected) or Far Red (infected) (Thermo Fisher Scientific) according to the manufacturer's instructions. Cells were mixed in a 1:1 proportion, and 4×10^9 RBC were transferred i.v. in the tail vein to noninfected recipients. Two hours after the transfer, blood was collected by retro-orbital bleeding to enumerate the percentage of each type of RBC transferred by FACS. At 2 and 7 d posttransfer, mice were euthanized and blood was collected to determine the percentage of remaining labeled RBC.

BrdU treatment

Mice were injected i.v. in the lateral tail vein with 1 mg of BrdU (100 μl of a 10 mg/ml solution; Becton Dickinson) at 1 wk, 24 and 12 h before sacrifice. For the 1-wk BrdU treatment, mice were additionally fed with 1 mg/ml BrdU in the drinking water. For 12 and 24 h chase, mice were injected only with BrdU i.v. and no chemical was provided in the drinking water.

Quantification of the bacterial load

A portion of liver and spleen was weighed and then homogenized in water containing 0.05% Tween 80. Tibiae BM was flushed with 1 ml of water. Homogenates were serially diluted in water containing 0.05% Tween 80 and plated in Middlebrook 7H10 Agar medium (BD Difco) supplemented with Oleic Acid–Albumin–Dextrose–Catalase. The plates were incubated at 37˚C until colonies were ready to count.

Hematological parameters

One hundred and fifty microliters of blood was collected to EDTA tubes (BD Vacutainer), and the remaining was let to clot and spun at high speed to collect serum. Blood and serum parameters were blindly analyzed in a certified laboratory (CoreLab, Centro Hospitalar do Porto, Porto, Portugal). The analysis was performed using a Sysmex XE-5000 hematology analyzer.

Histology and microscopy

Femurs were fixed in 10% neutral buffered formalin solution overnight at 4˚C, decalcified in EDTA/glycerol solution for 3 wk at 4˚C, and then included in paraffin blocks. Five-micrometer-thick sections were cut, deparaffinized, and processed through downgraded alcohols and rehydrated.

Perls staining. To detect ferric iron, sections were incubated in a 2% potassium ferrocyanide trihydrate/2% HCl solution for 30 min. Sections were rinsed five times in water.

Immunohistochemistry of F4/80 and Ziehl-Neelsen stain. Sections were deparaffinized and processed as described before. To unmask the antigenic epitope, sections were incubated in citrate buffer (pH 6) (Thermo Fisher Scientific) in a steamer for 20 min and allowed to cool for 10 min at room temperature (RT), followed by enzymatic digestion with 0.05% Trypsin (Life Technologies) in a humidified chamber at 37˚C for 30 min. Enzymatic reaction was stopped with incubations in cold water for 5 min, twice. After blocking endogenous peroxidase activity using Ultravision Hydrogen Peroxide Block (Thermo Fisher Scientific), endogenous biotin was blocked (Lab Vision Avidin Biotin Blocking Solution; Thermo Fisher Scientific). Unspecific binding sites were blocked with Normal Goat Serum (1:5 dilution; DAKO) in Ab diluent (Thermo Fisher Scientific) at RT for 30 min. Rat anti-mouse F4/80 Ab (clone BM8; BioLegend) was added to the sections and incubated in a humidified chamber overnight at 4˚C. Then, sections were stained with a biotinylated goat anti-rat IgG (Enzo) in a humidified chamber at RT for 30 min, followed by incubation with Streptavidin-HRP (Vector Laboratories) in a humidified chamber at RT for 30 min. DAB Quanto (Thermo Fisher Scientific) was added to allow the color development for 3 min. Slides were stained with Carbol Fuchsin and then heated and rinsed off in tap water. Then, 1% of hydrochloric acid in methanol was added to the slides. Slides were counter stained with hematoxylin, rinsed twice with water, dehydrated (reverse of downgraded alchools and deparaffinization), and coverslipped in Entellan. Sections were scanned in D-Sight Plus f2.0 and analyzed with D-Sight viewer.

Transmission electron microscopy. Tissues were fixed overnight at 4˚C in 4% formaldehyde and 1.25% glutaraldehyde in 0.1 M sodium cacodylate buffer (supplemented with 5 mM $MgCl_2$ and 5 mM $CaCl_2$; pH = 7.2), followed by postfixation with 1% osmium tetroxide in 0.1 M sodium cacodylate buffer for 1 h at RT and then with 1% uranyl acetate in water for 30 min. Tissues were gradually dehydrated in ethanol (25–100%), included with propylene oxide, and embedded in Epon resin. Ultrathin sections were stained with uranyl citrate and lead citrate and examined using a Jeol JEM-1400 transmission microscope at 80 kV.

RNA isolation and quantitative real-time PCR

Total RNA was isolated from liver, spleen, kidney and BM using a PureLink RNA Mini Kit (Invitrogen). Liver and spleen samples were collected and snap frozen in liquid nitrogen. BM was flushed from femurs with 1 ml of DMEM supplemented with 2% FBS, HEPES, PenStrep, and L-glutamine (all from Invitrogen). Cells were spun, and the pelleted cells were snap frozen in liquid nitrogen. Samples were stored at −80˚C. cDNA was synthetized from the isolated RNA using the NZY First-Strand cDNA Synthesis Kit (NZYTech, Lisbon, Portugal). For quantitative PCR, the reactions were performed with iTaq Universal SYBER Green Master Mix (Bio-Rad Laboratories) in a CFX Real-Time PCR Detection System (Bio-Rad Laboratories). Relative expression of each gene was calculated by the $2^{\Delta\Delta CT}$ method normalized to the expression of *Gapdh*. Primers were purchased from STABVIDA, Lisbon, Portugal. Primer sequences are in Supplemental Table I.

Cytokine analysis in serum

TNF-α, IL-6, and IFNG levels were quantified using the BD Cytometric Bead Array Mouse Inflammation Kit (BD Biosciences). Briefly, undiluted serum samples were mixed with a PE detection reagent, and the mixture was incubated for 2 h at RT in the dark. Samples were washed, and the beads were resuspended in washing buffer. Acquisition was performed in a BD FACSCanto II (BD Biosciences), and data analysis for quantification of cytokines was performed in FCAP Array Software (BD Biosciences).

Iron quantification

Femurs were flushed with 1 ml of DMEM medium, and cell suspensions were immediately spun. The mass of cell pellets was measured, and a 65% weight/weight solution of super pure nitric acid was added. Digestion took place at RT for 4 d, when cell pellets were completely solubilized. Frozen spleen portions were dried for 24 h at 95˚C, and the dry mass was measured. Then, ultrapure water was added, and the concentration of iron in the sample was determined using atomic absorption spectrophotometry with flame atomization (AAnalyst 200; PerkinElmer). Total iron content per femur was calculated by interpolation in a calibration curve.

Flow cytometry

BM cells were isolated by flushing long bones in DMEM supplemented with 2% heat-inactivated FBS, 5% HEPES, L-glutamine, and PenStrep (all from Invitrogen). Spleens were dissociated to single-cell suspensions and then filtered through 70-μm nylon mesh. Cells were counted using the trypan blue (Sigma-Aldrich) exclusion assay.

Erythroid progenitor staining. Two million cells were plated and stained with anti-CD3 (clone 17A2; BioLegend), anti-CD19 (clone 6D5; BioLegend), anti-TER119 (BioLegend), anti-CD71 (clone C2; BioLegend), and anti-CD11b (clone M1/70; BioLegend) Abs for 30 min on ice.

Hematopoietic stem and progenitor cell staining. Five million cells were plated and stained with a lineage mixture (containing the following clones: 17A2, RB6-8C6, RA3-6B2, TER119, and M1/70; BioLegend), anti-CD135 (clone A2F10; BioLegend), anti-CD117 (clone 2B8; eBioscience), anti-Sca-1 (clone D7; BioLegend), anti-CD32/16 (clone 93; BioLegend), and anti-CD34 (clone RAM34; eBiosciences) for 30 min, on ice.

Macrophages staining. One million cells were plated and stained with anti-F4/80 (cloneBM8; BioLegend), anti-CD169 (clone 3D6.112; BioLegend), anti-CD115 (clone 3D6.112; BioLegend), anti-Gr1 (clone RB6-8C5; BioLegend), and TER-119 (BioLegend) for 30 min, on ice. Then, cells were washed and fixed with 2% PFA for 10 min at RT.

BrdU staining. Extracellular staining was performed as described before. Cells were fixed and permeabilized according to BrdU Kit (BD Biosciences) instructions, followed by incubation with DNase (BD Biosciences) at 37˚C for 1 h. Cells were then stained with FITC-conjugated anti-BrdU (BD Biosciences) for 30 min at RT.

Peripheral blood staining and biotin detection. Blood was collected and mixed with an equal volume of a solution of K3EDTA and spun at 400 × *g* for 10 min. Cells were mixed with FACS buffer (1× PBS containing 2% BSA, 1 mM EDTA, and 0.1% sodium azide) and counted in a hemocytometer. Two million cells were plated and stained with anti-mouse CD47 (clone miap30; BioLegend), anti-TER119 (BioLegend), and anti-CD71 (clone C2; BD Pharmingen) for 30 min, on ice. For RBC turnover experiments, cells from mice previously injected with biotin (see details above) were also stained with a saturating amount of Alexa Fluor 488–conjugated Streptavidin (BioLegend). Cells were analyzed using a BD FACS Canto II flow cytometer and FlowJo.

Statistics

Student two-tailed *t* test and one-way ANOVA were performed using GraphPad Prism 7 (GraphPad Software, La Jolla, CA). A p value <0.05 was considered significant.

Results

Mycobacterial infection induces a hepcidin-independent microcytic anemia, alterations in the BM cellularity, and splenic erythropoiesis

To characterize the development of anemia during mycobacterial infection, C57BL/6 mice were infected with *M. avium* 25291 SmT by the i.v. route. As described previously (14, 27), this highly virulent strain grows exponentially in the liver and spleen of infected mice, at a higher rate in the first 4 wk p.i. and a bit slower thereafter. Groups of mice were sacrificed for hematological analysis at 4 and 8 wk p.i., times at which the animals did not lose more than 15% of the initial weight and did not show significant behavior alterations. At 4 wk p.i., the hematocrit and hemoglobin values were decreased (Fig. 1A, 1B). At 8 wk p.i., there was a significant decrease in the number of circulating RBC (Fig. 1C) as well as lower hematocrit and hemoglobin levels (Fig. 1A, 1B). Additionally, circulating RBC had reduced mean corpuscular volume (Fig. 1D), indicating that mycobacteria induced a microcytic anemia.

Because anemia related to chronic infections is usually associated with changes in serum iron levels (5, 6, 12, 13), we determined the amount of iron in the serum. Surprisingly, serum iron levels remained unchanged compared with that of noninfected mice at the time points analyzed (Fig. 1E). However, we observed a decrease in transferrin saturation, related to a higher total iron-binding capacity (an indirect measurement of total transferrin present in the serum) (Fig. 1F), suggesting that infection did not cause hypoferremia but could cause a reduced availability of the circulating iron. We also observed that the proinflammatory cytokines IFNG and TNF-α were increased in

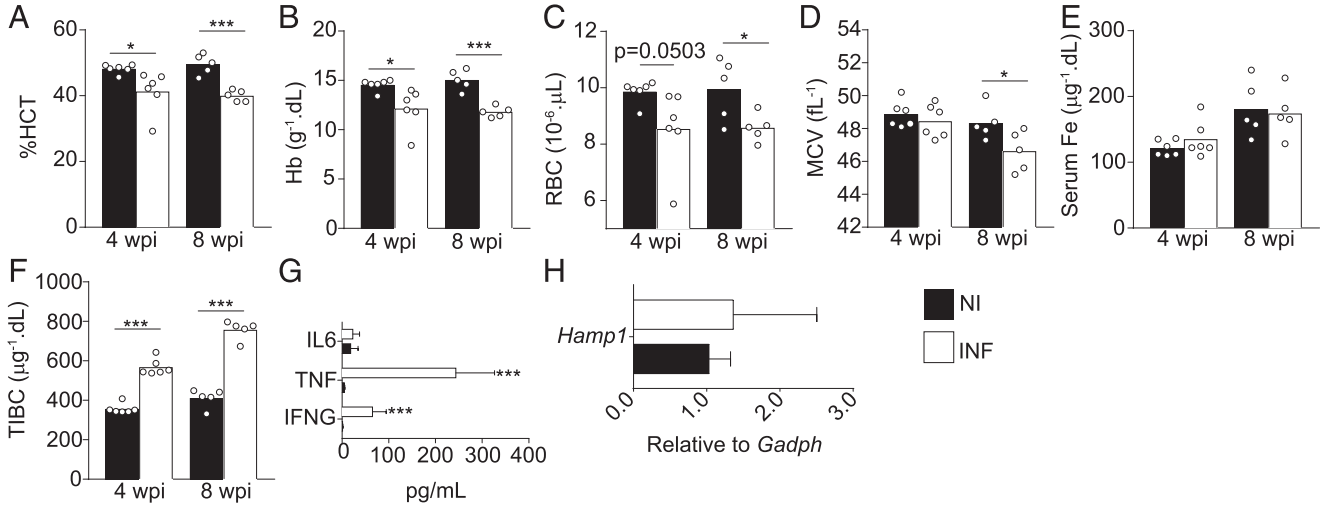

FIGURE 1. Mycobacterial infection triggers a hepcidin-independent microcytic anemia. (**A**–**D**) Quantification of hematocrit (A), hemoglobin (B), circulating RBCs (C), and their mean corpuscular volume (D) in the peripheral blood of *M. avium*–infected and noninfected mice at 4 and 8 wk p.i. (**E** and **F**) Quantification of serum iron (E) and total iron binding capacity (F) in the serum of infected and noninfected mice. Serum was obtained by centrifugation of peripheral blood. (**G**) Amount of IFNG, TNF, and IL-6 present in the serum of 8-wk-infected ($n = 5$) and noninfected mice ($n = 5$). (**H**) *Hamp1* mRNA levels relative to *Gapdh* in the liver of 8-wk-infected ($n = 5$) and noninfected ($n = 5$) controls. Bars represent the average of the experimental group, and dots represent each analyzed mouse. Black bars denote noninfected mice (NI). White bars denote infected mice (INF). Data are representative of at least three independent experiments. $*p < 0.05$, $***p < 0.001$ (unpaired, two-tailed Student *t*-test).

the serum of 8-wk-infected mice, but IL-6, an important inducer of alterations on iron metabolism, was not increased (Fig. 1G). Accordingly, we also did not detect an induction of the expression of hepcidin (the main regulator of iron metabolism) as measured by the levels of *Hamp1* mRNA in the liver (Fig. 1H).

The lower availability of iron in circulation could lead to impaired iron delivery to the BM for erythropoiesis. To investigate this, we quantified the amount of iron in the BM of infected and noninfected aged-matched mice. *M. avium*–infected mice showed reduced iron stores (Fig. 2A, 2B), suggesting a decrease of iron availability in the BM during infection, which could in turn lead to a blockade in erythroid development.

Previous studies demonstrated that *M. avium* infection dramatically shapes and changes the hematopoietic stem and progenitor cells (17, 18). We thus decided to thoroughly investigate the impact of infection on the BM cellularity and architecture. Because the presence of bacteria in the BM had not been evaluated before in our model, we started by quantifying CFUs in this tissue. Viable *M. avium* was present in BM, and the bacterial load increased over time as measured by the quantification of CFUs (Fig. 2C). The majority of the observed bacteria resided inside macrophages within the BM parenchyma (Fig. 2D).

The host BM total cell number was decreased by ~3-fold at 8 wk p.i. (Supplemental Fig. 1A). Similarly to previous reports, infection increased the frequency of mature hematopoietic (Lin^+) cells (Supplemental Fig. 1B) and also of hematopoietic stem ($CD34^{lo}Lin^-$ $Sca1^+$ $c\text{-}kit^+$) cells (Supplemental Fig. 1C). Interestingly, the frequency of BM macrophages [$Gr1^{lo}CD115^-F4/80^+$, as defined in (28)] was increased in infected animals at 4 wk, but at 8 wk p.i., it was not different from the noninfected controls (Fig. 2E). However, the frequency of macrophages of erythroblastic islands [defined as $Gr1^{lo}CD115^-F4/80^+CD169^+$ (19)] was decreased (Fig. 2F) in infected mice, suggesting that erythropoiesis could be impaired.

In fact, the frequency of the multipotent progenitors upstream of the erythroid lineage commitment, the MEP stage, was reduced in the BM of infected mice (Fig. 2G). We then investigated the different developing erythroid stages in BM, using the gating strategy shown in Fig. 2H. We found that the frequency of the earliest erythroid stage, Pro-E, was increased in infected mice (Fig. 2I), but that of the downstream progenitors, the different stages of erythroblasts, was decreased (Fig. 2J–L). Overall, our results suggested that the pool of Pro-E cells expanded at the expense of MEP during infection, but the downstream differentiation of these progenitors was impaired.

Because inflammation drives the mobilization of hematopoietic progenitors from the BM to the spleen (29, 30), we evaluated the erythroid development in the spleen of infected mice. As expected from previous observations (16, 27), mycobacteria actively proliferated in the spleen (Fig. 3A). We also observed splenomegaly (with an increase of spleen cellularity of ~7-fold) and disruption of the splenic architecture in mycobacteria-infected mice. Whereas the spleens of the noninfected mice show the typical histological organization in white and red pulp (Fig. 3B, left side), the spleens of infected mice have an altered histological architecture, becoming rich in granulomatous lesions and devoid of a clear separation between red and white pulp (Fig. 3B, right side). Similarly to the BM, the spleen of infected mice had a lower concentration of iron (Fig. 3C). However, the frequency of erythroid cells ($TER119^+$ cells) was increased in the spleen of infected mice (Fig. 3D) as well as the populations representing all the stages of erythroid development (Fig. 3E–H). Moreover, we detected a higher expression of erythropoiesis-related genes, such as hemoglobin (*Hbb-bs*) and transferrin receptor (*Tfr*) (Fig. 3I, 3J), indicating that splenic erythropoiesis occurred during mycobacterial infection.

Erythroid commitment and differentiation are not blocked during infection

To further understand whether the erythroid differentiation in the BM was blocked during mycobacterial infection, we determined the percentage of cells incorporating BrdU (%$BrdU^+$) after 1 wk, 24 h, or 12 h of BrdU administration (Fig. 4A). The dynamics of erythroid development can be studied by measuring the BrdU incorporation in hematopoietic progenitor cells. BM cells were gated as depicted in Fig. 2H, and the percentage of $BrdU^+$ cells was determined for each population. $BrdU^+$ cells are proliferating

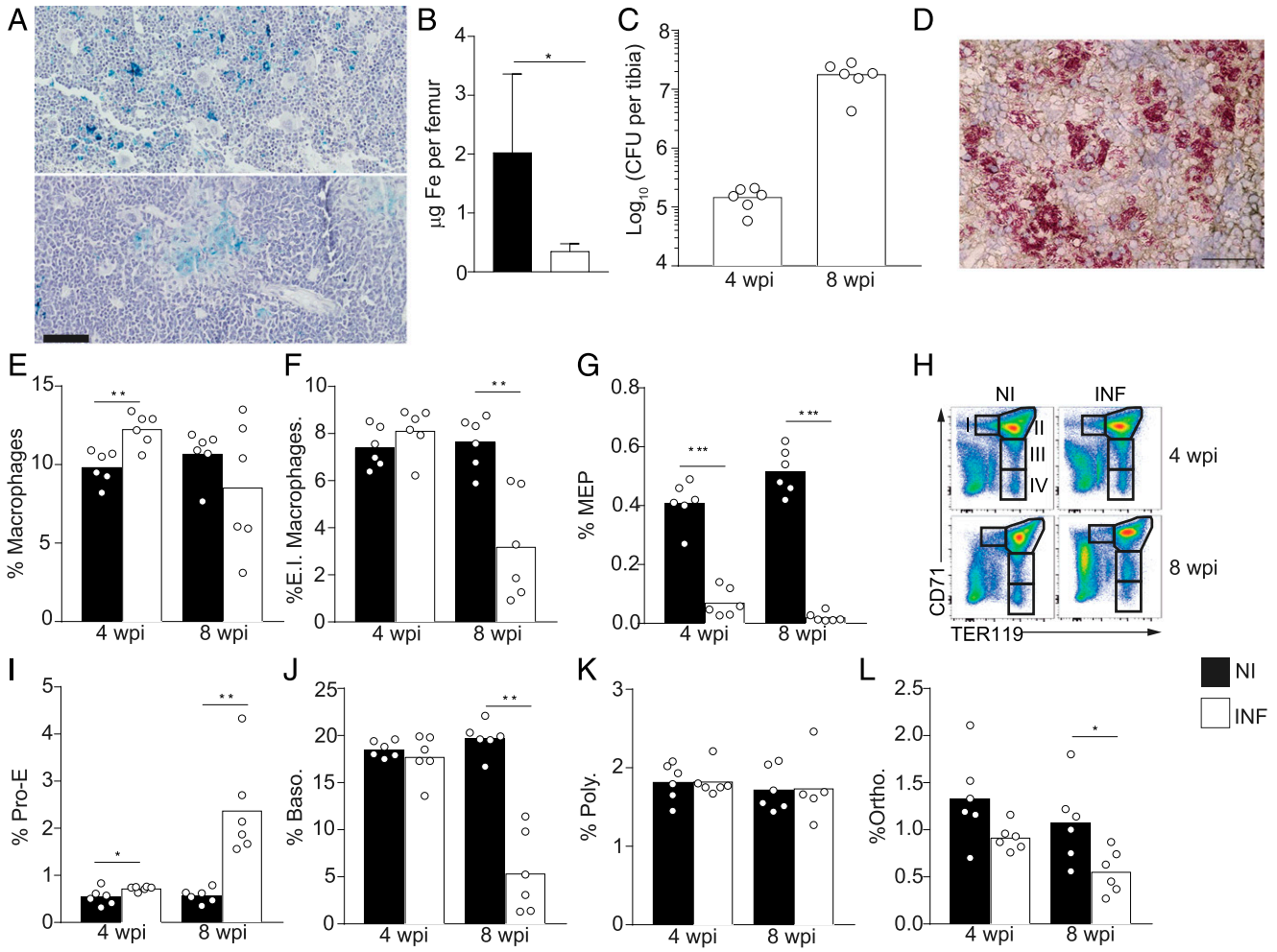

FIGURE 2. *M. avium* infection induces alterations in BM architecture and cellular composition. (**A**) Five-micrometer-thick section of Perls stained femurs from noninfected (upper panel) and *M. avium*–infected (lower panel) mice. Scale bar, 200 μm. (**B**) Total amount of iron in BM. Bars represent the average of the experimental group ($n = 3$), and error bars indicate SD. (**C**) Bacterial load in tibias of mice infected for 4 and 8 wk. (**D**) Immunohistochemistry for F4/80 (dark brown) and Ziehl-Neelsen staining of mycobacteria (red) of 5-μm-thick sections of 8-wk-infected mice. Scale bar, 50 μm. (**E**) Frequency of $Gr1^{low}CD115^{-}F4/80^{+}$ macrophages. (**F**) Frequency of $Gr1^{low}CD115^{-}F4/80^{+}CD169^{+}TER119^{+}$ macrophages in erythroblastic islands. (**G**) Frequencies of $Lin^{-}cKit^{+}Sca1^{-}CD34^{-}CD16/32^{-}$ MEP cells in BM. (**H**) Gating strategy of erythroid progenitors in BM using the surface expression of TER119 and CD71. Cells were negatively gated for CD19, CD11b, and CD3 and identified according to their surface expression of TER119 and CD71, as follows: gate I, Pro-E population; gate II, basophilic erythroblasts; gate III, polychromatic erythroblasts; and gate IV, orthochromatic erythroblasts. (**I–L**) Frequencies of erythroid progenitors in BM: Pro-E (I), basophilic erythroblasts (J), polychromatic erythroblasts (K), and orthochromatic erythroblasts (L). Black bars denote noninfected mice (NI). White bars denote infected mice (INF). Bars represent the average of the experimental group, and dots represent each analyzed mouse. Data are representative of three independent experiments. $*p < 0.05$, $**p < 0.01$, $***p < 0.001$ (unpaired, two-tailed Student *t* test).

cells that incorporate BrdU while differentiating. A continuous incorporation of BrdU for 1 wk allows us to understand whether the commitment to and the progression in the erythroid lineage is affected during infection. When analyzing the earliest stages, Pro-E and basophilic erythroblasts (Fig. 4B), we observed that after 1 wk of continuous BrdU administration, more than 95% of the cells were $BrdU^{+}$, and we did not detect differences between infected and noninfected mice. However, the $\%BrdU^{+}$ cells in the latest stages of erythroblast development (especially orthochromatic erythroblasts) was higher in infected animals (Fig. 4B). Of note, this long-term BrdU administration did not reveal differences in incorporation by HSC, multipotent progenitors (MPP), and MEP between infected and noninfected mice (Supplemental Fig. 1D), indicating that long-term precursor transition to the MEP stage was not impaired by infection.

To investigate whether higher BrdU incorporation in the later stages of differentiation was due to a faster erythroid development or to a blockade in erythropoiesis, we analyzed the $\%BrdU^{+}$ cells after 24- and 12-h pulses. For these timepoints, mice were injected i.v. with BrdU, and no chemical was provided in the drinking water. In both cases, we detected no difference in the $\%BrdU^{+}$ cells in the earlier stages of erythropoiesis, but the latest stage of erythroblast differentiation (orthochromatic erythroblasts) had a higher incorporation of BrdU in infected mice (Fig. 4C). With a shorter BrdU incorporation period (12 h), an additional decrease in $\%BrdU^{+}$ polychromatic erythroblasts was observed (Fig. 4D). Interestingly, with this short pulse, HSC and MPP in infected mice had ~2-fold more BrdU incorporation than noninfected controls, but the percentage of BrdU incorporation in MEP was similar between infected and noninfected mice (Supplemental Fig. 1D).

Overall, the data indicate that although *M. avium* affects the proliferation of HSC and MPP, it does not affect the commitment to the erythroid lineage. Moreover, erythropoiesis proceeds normally until the later stages of erythroblast, at the transition

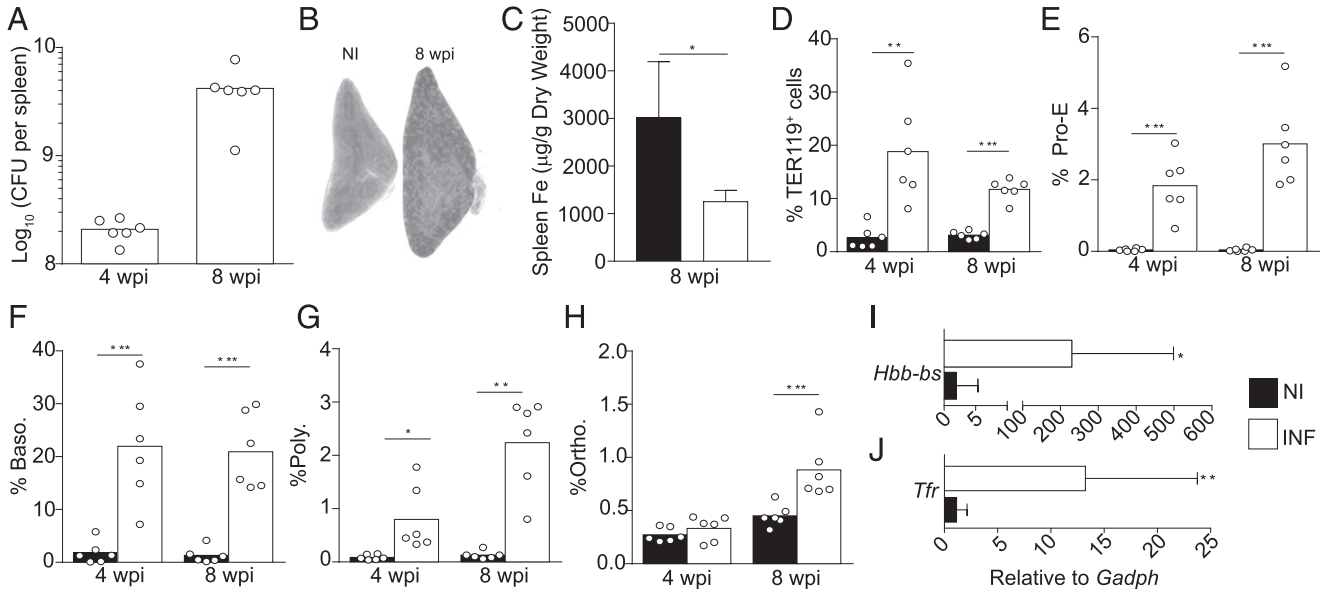

FIGURE 3. Mycobacteria infection mobilizes erythroid progenitors to the spleen. (**A**) Bacterial load in the spleen (measured by CFU assay) at 4 and 8 wk p.i. (**B**) Five-micrometer-thick H&E-stained spleen sections, illustrating the structural alterations caused by infection. (**C**) Total amount of iron in spleen. Bars represent the average of the experimental group (n = 5), and error bars indicate SD. (**D**) Frequency of total TER119$^+$CD3$^-$CD19$^-$ cells. (**E**–**H**) Frequencies of developing erythroid stages in the spleen: Pro-E (E), basophilic erythroblasts (F), polychromatic erythroblasts (G), and orthochromatic erythroblasts (H). (**I** and **J**) Splenic mRNA levels of *Hbb-bs* (I) and *Tfr* (J) at 8 wk p.i. *Gapdh* was used as housekeeping gene. Black bars denote noninfected mice (NI). White bars denote infected mice (INF). Bars represent the average of the experimental group (n = 10), and dots represent each analyzed mouse. $*p < 0.05$, $**p < 0.01$, $***p < 0.001$ (unpaired, two-tailed Student t test).

from polychromatic to orthochromatic erythroblasts, when this differentiation seems to occur at a faster pace. This is further supported by the observation of an increase in circulating reticulocytes during mycobacterial infection (Fig. 4E). Of note, the transcription of hemoglobin and erythropoietin receptor genes in BM was not affected during infection (Supplemental Fig. 1E).

During mycobacterial infection, RBC have a shorter half-life

Although the formation of new erythrocytes was not blocked during infection, the quality of the cells formed could be compromised. In fact, circulating erythrocytes had lower mean corpuscular hemoglobin (Fig. 5A), and *M. avium*–infected mice had a higher percentage of TER119$^+$CD71$^+$ cells within circulating RBC population in the blood (Fig. 5B), indicating the early egress of developing erythrocytes to circulation. We hypothesized that the faster erythropoiesis resulted in poorly formed RBC that would have a shorter life span. To assess that, mice were injected with biotin 14 d prior to their sacrifice. Two hours after biotin injection, 95.60 ± 1.14% of RBC were labeled with biotin. Fourteen days later, 70.75 ± 1.48% of RBC remained biotin labeled in control noninfected mice, whereas only 43.65 ± 14.78% of the RBC remained biotin labeled in infected mice (Fig. 5C), indicating a faster removal of RBC from circulation during

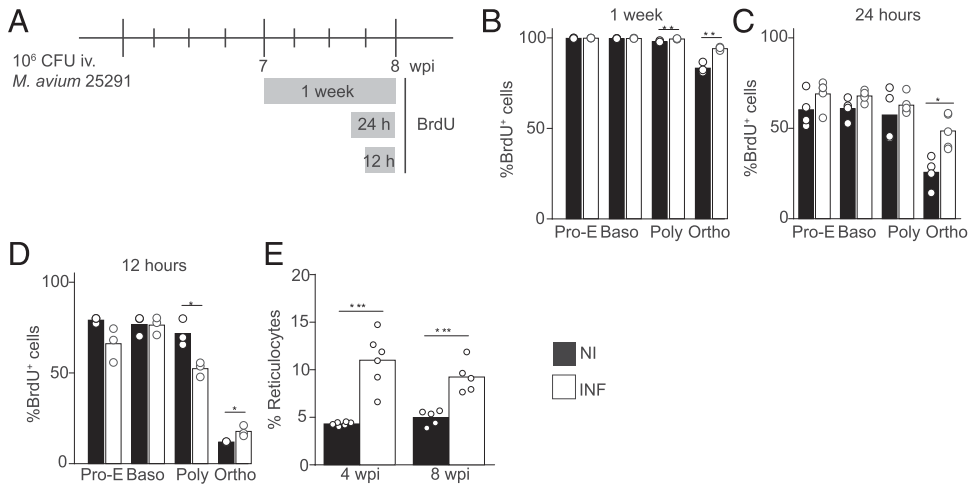

FIGURE 4. Erythroid commitment and differentiation are not blocked during mycobacteria infection. (**A**) Scheme representing the BrdU assay. Mice were pulsed with 1 mg of BrdU i.v. for 1 wk, 24 h, or 12 h. Mice were sacrificed at 8 wk p.i. At least four mice for each experimental group (infected and noninfected) were used at each time point. (**B**–**D**) Percentage of BrdU$^+$ cells in developing erythroid stages after 1 wk (B), 24 h (C), and 12 h (D) after BrdU administration. (**E**) Percentages of circulating reticulocytes relative to RBC in peripheral blood. Bars represent the average of the experimental group, and dots represent each analyzed mouse. $*p < 0.05$, $**p < 0.01$, $***p < 0.001$ (unpaired, two-tailed Student t test).

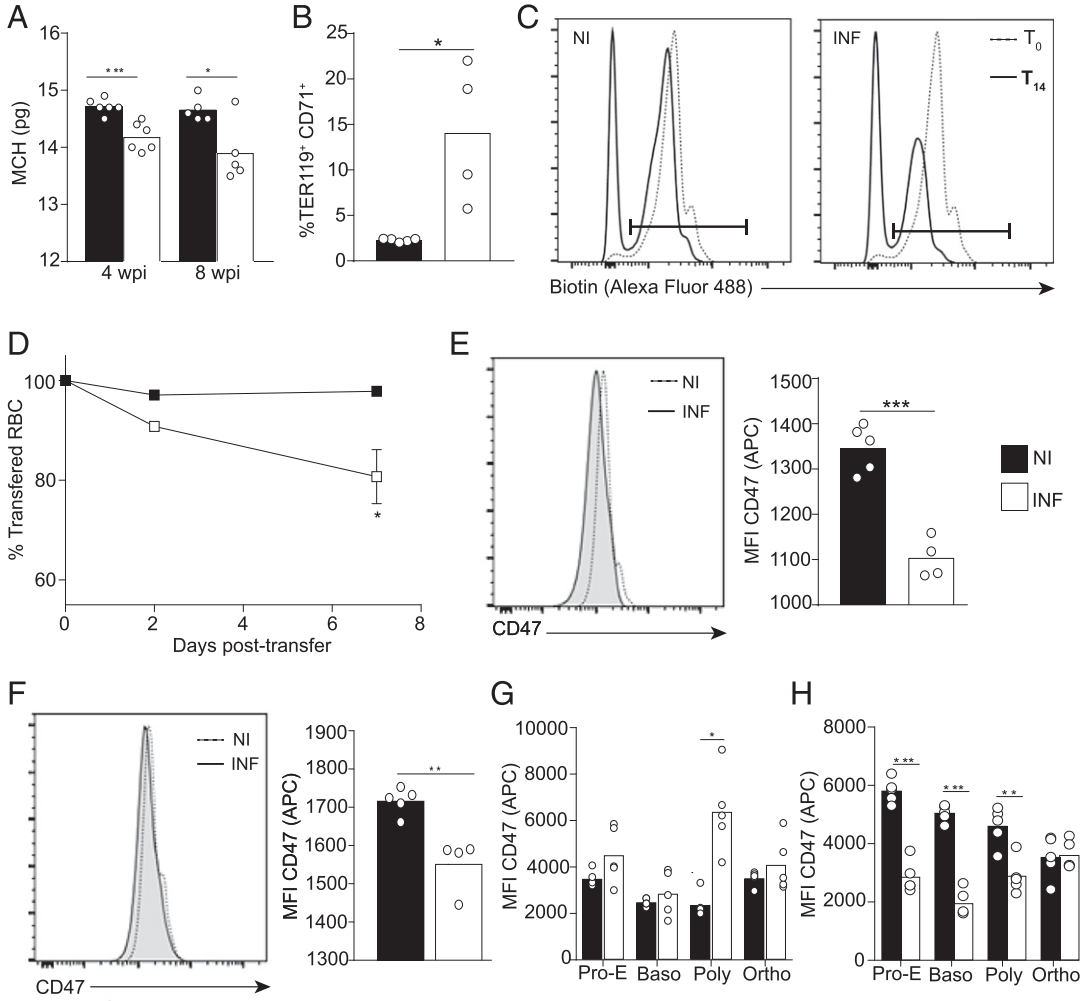

FIGURE 5. During mycobacterial infection, RBC have a shorter half-life. (**A**) Mean corpuscular hemoglobin (MCH) in peripheral blood. (**B**) Percentage of developing erythrocytes (defined as $TER119^+CD71^+$ cells) in peripheral blood. (**C**) Percentage of biotinylated $TER119^+$ cells in the blood at 2 h (T0, dotted lines) and 14 d (T14, filled lines) after biotin i.v. injection in noninfected (left panel) and 8-wk *M. avium*–infected (right panel) mice. Black bars denote noninfected mice (NI). (**D**) Percentage of RBC transferred from infected and noninfected donors in the circulation of noninfected recipients at different time points after the adoptive transfer. (**E**–**H**) CD47 MFI in circulating mature erythrocytes (D), circulating developing erythrocytes ($TER119^+CD71^+$) (E), erythroid progenitors in BM (F), and erythroid progenitors in spleen (G). Black bars denote NI. White bars denote infected mice (INF). Bars represent the average of the experimental group, and dots represent each analyzed mouse. Each group contained at least three animals. $*p < 0.05$, $**p < 0.01$, $***p < 0.001$ (unpaired, two-tailed Student *t* test).

mycobacterial infection. To confirm an intrinsic short life of the RBC in infected mice, we labeled RBC from infected and noninfected mice with different probes, mixed the cells at a 1:1 proportion, and transferred them to noninfected recipient mice. A significantly decreased percentage of RBC from infected donors remained in circulation 7 d after transfer, compared with the RBC coming from noninfected donors (Fig. 5D).

Because CD47 downregulation on the cell surface is involved in the recognition and removal of aged cells, we evaluated the surface expression of CD47. Both developing and mature RBC in circulation in infected mice expressed slightly (but statistically significant) lower levels of CD47 compared with noninfected controls (Fig. 5E, 5F), indicating they were more prone to removal by phagocytosis. To determine whether the lower expression of CD47 was due to cell-intrinsic defects during development, we measured the expression of CD47 in erythrocyte precursors in BM and spleen. Whereas the different stages of developing erythrocytes in BM did not show reduced CD47 expression (Fig. 5G), splenic developing erythrocytes had lower expression of CD47 (Fig. 5H). Moreover, in the biotin-labeling assay, we observed that the nonbiotinylated (recently formed) RBC in circulation in infected mice had lower CD47 expression (CD47 mean fluorescence intensity [MFI]: 2880 ± 18) compared with noninfected mice (CD47 MFI: 3092 ± 258).

Infection by mycobacteria increases erythrophagocytosis, most notably in the liver

Our data indicated that during chronic infection, erythrocyte removal was accelerated. The liver has been identified as the primary organ responsible for erythrophagocytosis in conditions of poor erythrocyte integrity (25). It is also the main target organ during systemic mycobacterial infection, becoming fibrotic and rich in granulomas (Fig. 6A, bottom panel) (31). To evaluate whether erythrocytes were removed by the liver during mycobacterial infection, we quantified erythrophagocytosis events using transmission electron microscopy (TEM). Whereas in the noninfected controls, erythrocytes were found mostly extracellular or inside blood vessels (Fig. 6B, top panel delimited area), in infected mice, erythrocytes were mostly inside cells, some of which could be identified as macrophages based on the morphology of the nuclei (Fig. 6B, bottom panel asterisks and Fig. 6C). In addition, the liver of infected mice expressed higher levels of *SpiC* and *Hmox1*

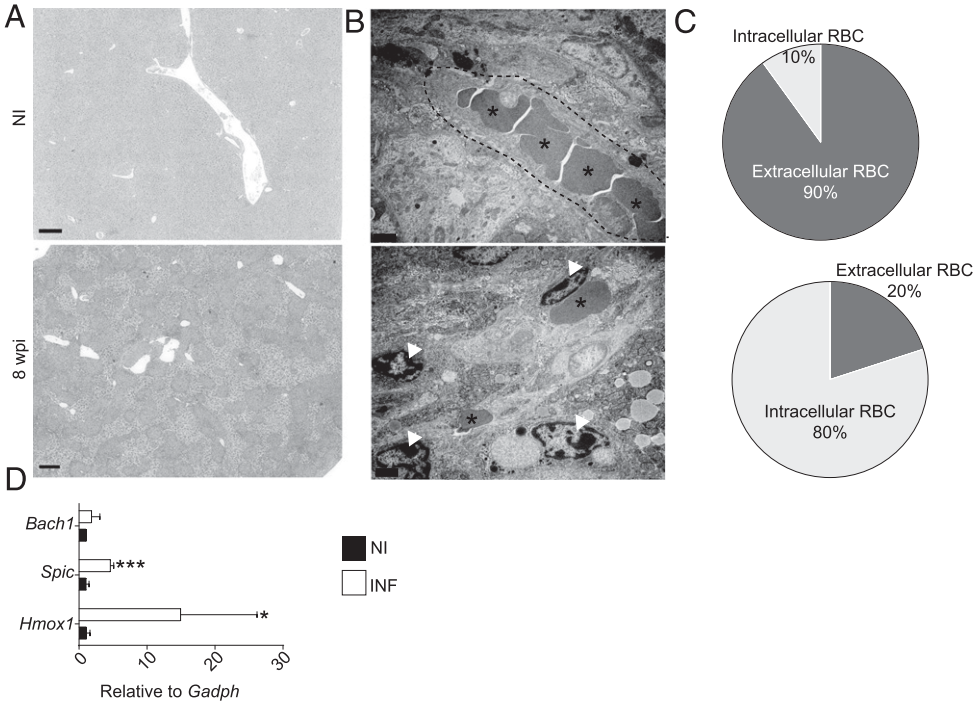

FIGURE 6. Infection by mycobacteria increases erythrophagocytosis. (**A**) Low-magnification micrographs of H&E-stained liver sections of noninfected (upper panel) and 8-wk-infected mice (lower panel). Scale bar, 500 μm. (**B**) Ultrathin liver sections showing erythrocytes (denoted by an asterisk [*]) predominantly inside vessels (labeled by the dash lines) in noninfected mice (upper panel) and predominantly inside cells in *M. avium*–infected mice at 8 wk of infection (lower panel), as shown by the arrowheads labeling nuclei. Scale bar, 2 μm (**C**) Percentage of intracellular versus extracellular erythrocytes in livers of noninfected (upper plot) and 8-wk-infected mice (lower plot). (**D**) Expression of *Bach1*, *Spic*, and *Hmox1* genes relative to *Gapdh* in the livers of noninfected mice (NI, black bars) and infected mice (INF, white bars) at 8 wk p.i. Bars indicate the average of each group, and error bars represent SD. Ten mice were analyzed per condition. Bars represent the average of the experimental group, and dots represent each analyzed mouse. $*p < 0.05$, $***p < 0.001$ (unpaired, two-tailed Student *t* test).

genes, which are involved in iron recycling, but unchanged expression of *Bach1*, as this transcription factor is posttranscriptionally regulated (Fig. 6D).

IFNG-dependent reticulocytosis and erythrophagocytosis are key to infection-induced anemia

Our data indicated that mycobacteria-induced anemia is a consequence of an accelerated erythropoiesis and increased erythrophagocytosis. IFNG has been reported to block hematopoiesis during *M. avium* infection (17, 18) and to induce erythrophagocytosis due to hyperactivation of macrophages (32). To evaluate the contribution of IFNG to the development of anemia during mycobacterial infection, we infected *Ifng*-deficient mice, MIIG mice, and wild-type (WT) littermate controls for 8 wk. Whereas *Ifng*-deficient mice cannot produce IFNG, MIIG mice have macrophages insensitive to IFNG, by expressing a dominant negative mutant IFNG receptor in $CD68^+$ cells (26). Although IFNG is a protective cytokine during mycobacterial infection, *M. avium* 25291 SmT strain was previously reported to resist IFNG-mediated protection (16). Accordingly, 8 wk p.i., the bacterial loads were similar in mice with the three genotypes in the liver (WT: $2.4 \pm 1.6 \times 10^{10}$; $Ifng^{-/-}$: $9.7 \pm 2.8 \times 10^9$; MIIG: $1.5 \pm 0.5 \times 10^{10}$), spleen (WT: $8.9 \pm 7.9 \times 10^9$; $Ifng^{-/-}$: $6.8 \pm 1.8 \times 10^9$; MIIG: $6.1 \pm 6.2 \times 10^9$), and BM (WT: $1.9 \pm 1.3 \times 10^7$; $Ifng^{-/-}$: $2.0 \pm 1.1 \times 10^7$; MIIG: $1.3 \pm 0.8 \times 10^7$). Additionally, circulating IFNG was absent in *M. avium*–infected $Ifng^{-/-}$ mice but present in MIIG mice, although at reduced levels as compared with WT littermates (Fig. 7A). Thus, both *Ifng*-deficient and MIIG mice are good models to study the development of anemia in response to infection without increased bacterial loads, which could independently affect the host response. Because of the implications of IFNG in the early stages of hematopoiesis, we analyzed the erythroid development in the BM of $Ifng^{-/-}$. Corroborating previous works (17), in the absence of IFNG, infection did not lead to increased frequency of HSC, and the frequencies of MEP and downstream erythroid progenitors were similar to noninfected mice (Supplemental Fig. 2A–F). However, we observed increased splenic frequencies of all erythroblast populations in infected $Ifng^{-/-}$ mice (Supplemental Fig. 2G–J), indicating that the mobilization of erythroid progenitors to the spleen is independent of IFNG.

Moreover, we found that the percentage of circulating immature erythrocytes and that of reticulocytes was not altered by infection in $Ifng^{-/-}$, in clear contrast with WT and MIIG mice, which exhibited infection-associated reticulocytosis (Fig. 7B, 7C). These results indicate that IFNG drives an increased erythropoietic output during mycobacterial infection, instead of blocking erythropoiesis, as suggested by previous reports (18). The data further support a role for IFNG as contributing for anemia development during mycobacterial infection through alterations in erythropoiesis.

Next, we investigated whether IFNG affects erythrophagocytosis by activating macrophages to phagocytose RBC. We analyzed the liver of infected and noninfected *Ifng*-deficient and MIIG mice by TEM to enumerate intracellular and extracellular RBC. In WT mice, infection increased by 8-fold the percentage of intracellular RBC (Fig. 6B). IFNG-insensitive macrophages could engulf RBC as much as IFNG-activated macrophages (Fig. 7D). This finding highly suggests that IFNG activation of macrophages is not a determinant signal required for the increased removal of RBC. Yet, erythrophagocytosis was not increased in $Ifng^{-/-}$ mice during infection (Fig. 7E). Supporting the notion of increased RBC

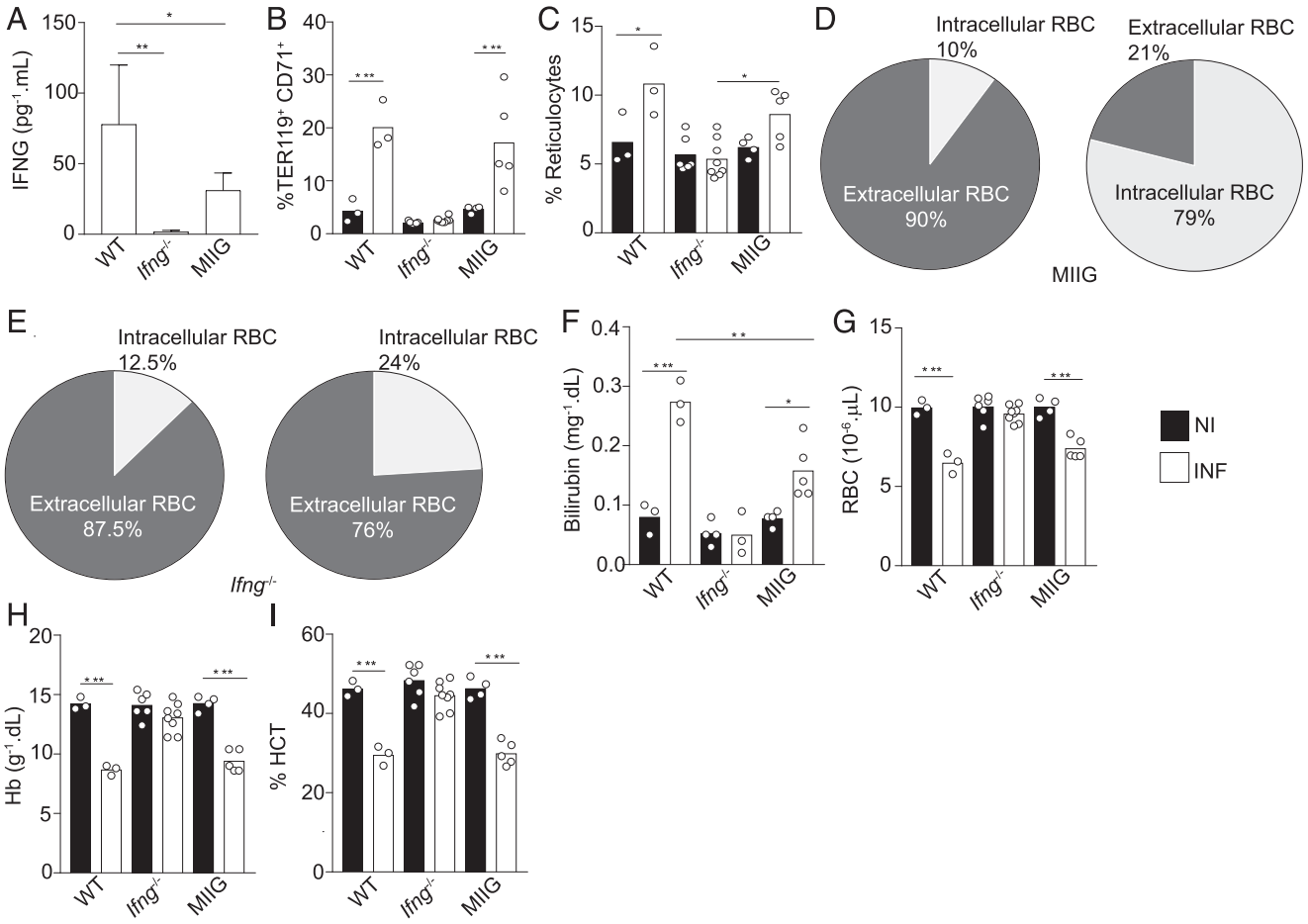

FIGURE 7. IFNG induces reticulocytosis, premature release of immature erythrocytes to circulation, and increased erythrophagocytosis, independently of its sensing by macrophages. (**A**) Amounts of serum IFNG in WT, *Ifng*$^{-/-}$, and MIIG mice at 8 wk p.i. (**B**) Percentage of TER119^{+} CD71^{+} cells in peripheral blood. (**C**) Percentage of circulating reticulocytes. (**D**) Percentage of intracellular versus extracellular erythrocytes in livers of noninfected (left plot) and in 8-wk-infected MIIG mice (right plot). (**E**) Percentage of intracellular versus extracellular erythrocytes in livers of noninfected (left plot) and in 8-wk-infected *Ifng*$^{-/-}$ mice (right plot). (**F**) Amount of total bilirubin in the serum. (**G–I**) Enumeration of circulating RBCs (G), hemoglobin (H), and hematocrit (I) in peripheral blood of *M. avium*–infected (INF, white bars) and noninfected (NI, black bars) WT, *Ifng*$^{-/-}$, and MIIG mice. Bars indicate average, and each dot corresponds to each analyzed sample. At least three mice were used in each experimental group. $*p < 0.05$, $**p < 0.01$, $***p < 0.001$ (one-way ANOVA).

degradation during infection, WT and MIIG but not *Ifng*$^{-/-}$ mice had increased levels of circulating bilirubin (Fig. 7F). Whereas MIIG and WT mice had reticulocytosis and anemia, *Ifng*-deficient mice did not show reticulocytosis (nor increased erythrocyte removal) and thus did not develop anemia (Fig. 7G–I).

Together, the data suggest that mycobacteria-induced anemia results from IFNG-driven reticulocytosis, RBC-intrinsic alterations, and increased erythrocyte degradation.

Discussion

In this study, we show that mycobacteria-induced anemia depends on IFNG and is mainly caused by a decreased erythrocyte life span, a component that has not been valued by any previous studies in this field. We found that erythropoiesis was enhanced in response to mycobacterial infection, as indicated by the increased numbers of developing erythrocytes and reticulocytes in circulation. However, erythrocytes formed during infection had intrinsic defects, such as reduced size, lower amount of hemoglobin, and lower expression of CD47 at the cell surface. Notably, the life span of circulating erythrocytes was decreased in *M. avium*–infected mice, and a significant increase in erythrophagocytosis in the liver was observed.

Erythropoiesis is the major consumer of iron in the body (33), and when iron levels fall below a certain threshold, erythroid progenitors stop their proliferation and progression through the different stages of erythroid development (34–36). However, in this study, we did not find a reduced proliferation of erythroid progenitors during infection nor altered erythropoietin receptor expression in BM, despite the decrease in iron concentration in the tissue. Our findings suggest that iron redistribution in response to *M. avium* infection does not alter the above-mentioned mechanisms of iron sensing and regulation of erythropoiesis.

During *M. avium* infection, erythropoiesis was actually enhanced both in the BM and in the spleen. Splenic erythropoiesis could be due to compensatory mechanisms aimed at the correction of initial stages of anemia or could directly result from inflammatory signals. The early release of hematopoietic progenitors from the BM to the spleen during inflammatory conditions has been described before (29, 30). The observation of granulomatous-type lesions containing mycobacteria suggested a local inflammatory state in the BM. Additionally, we found markers of systemic inflammation, such as high levels of INFG and TNF (although not of IL-6), in the serum of infected mice. Of note, mobilization of erythroid progenitors from the BM to the spleen was not mediated by IFNG, indicating that

multiple factors contribute to the hematopoietic alterations observed during mycobacterial infections.

IFNG has been described as the major dysregulator of hematopoiesis during mycobacteria infection by inducing the overproliferation of HSC, skewing hematopoiesis toward myelopoiesis and leading to HSC depletion (17, 18). Interestingly, our data showed that despite the increase in the number and proliferation of HSC, the commitment to and progression in the erythroid lineage was not affected. We also failed to detect pancytopenia as we had normal numbers of leukocytes in circulation, suggesting that the establishment of anemia is independent of the previously described changes in the early hematopoietic compartment and occurs before the establishment of more-dramatic changes in the hematopoietic compartment. Nevertheless, our results pointed to a key role of IFNG during infection. IFNG induced reticulocytosis and the release of immature erythroid progenitors to the circulation.

CD47 is often considered a "don't eat me" signal, which by binding to its receptor SIRPa (expressed in myeloid cells) controls phagocytosis (37). Although CD47 is expressed in almost every cell, its levels may fluctuate during an immune response. For instance, the expression of CD47 on hematopoietic stem and progenitor cells increases upon cytokine-induced mobilization of the cells from BM to circulation (38). The augmented expression of CD47 may be important to reduce phagocytosis of the cells. Besides multipotent progenitors, T cell progenitors also express high levels of this receptor (39). In hemophagocytic lymphohistiocytosis syndromes, CD47 is selectively downregulated in HSC, which are then more susceptible to phagocytosis (40). Yet, in the present work, erythrocyte precursors in BM had normal levels of CD47. Immature and mature circulating erythrocytes, on the contrary, expressed lower levels of CD47 during mycobacterial infection, suggesting that a downregulation of CD47 occurs in circulation or it may be a trait of spleen-derived cells, as erythrocyte precursors in the spleen had indeed a significant decrease of CD47 surface expression.

In agreement with the reduced erythrocyte life span, our data also pointed to increased erythrophagocytosis in the liver, with upregulation of iron-recycling genes and increased serum bilirubin. In situations of increased erythrocyte damage, hepatic macrophages assume the control of erythrocyte disposal and iron recycling (25). Damaged erythrocytes are contained in erythrophagolysosomes, where they are degraded. Degradation of erythrocytes leads to degradation of hemoglobin, releasing heme. Heme is exported to the cytosol, where HMOX1 removes iron from protoporphyrin. The recycled iron is then either stored in ferritin or exported by ferroportin for reuse (41). Heme also activates the heme-binding transcriptional repressor BACH1 and subsequently induces the transcription factor SPI-C, which will induce the differentiation of monocytes and resident macrophages into iron-recycling cells. The hallmark of these cells is the expression of HMOX1 (42). We have previously described that *M. avium* infection causes upregulation of HMOX1 in tissues and that *Hmox1*-deficient mice are highly susceptible to infection because of a higher amount of circulating heme and hepatic damage (15). Together with the present work, these results suggest that *M. avium* infection causes massive erythrophagocytosis. On one hand, this will lead to the release of high amounts of heme, which is toxic for the host and contributes to susceptibility to infection. On the other hand, this is a major contributor to the development of anemia.

In addition to the lower expression of CD47 at the surface of erythrocytes, the enhanced eagerness of macrophages to take them up may be caused by systemic inflammation. In a previous in vitro study, it was shown that *Salmonella*-infected BM-derived macrophages were more prone to phagocytize erythrocytes through a TLR4-dependent pathway (43). In contrast, continued infusion of IFNG in vivo led to increased erythrophagocytosis and anemia, which were dependent on IFNG signaling in macrophages (32). Hemophagocytes are myeloid cells with increased avidity to engulf erythrocytes and, in some instances, leukocytes. These cells are frequently observed during infections by pathogens as *Salmonella enterica*, *Brucella abortus*, EBV, and *M. tuberculosis*; and the number of cases reporting the appearance of these cells in response to infection is increasing (44–47). Proinflammatory cytokines such as IFNG and TNF may orchestrate macrophages to phagocytose erythrocytes (48–49). However, in the current study, mice with macrophages insensitive to IFNG (MIIG mice) showed increased erythrophagocytosis and developed anemia, suggesting that the erythrophagocytosis during infection was not directly triggered by IFNG-induced macrophage activation. Additionally, when we transferred erythrocytes from infected and noninfected mice to normal, noninfected recipients, we observed that the former had a shorter time in circulation than the latter, further indicating that the increased erythrophagocytosis is due to erythrocyte-intrinsic alterations occurring during infection and not to an increased eagerness of the macrophages from infected mice.

Yet, the development of anemia during *M. avium* infection was dependent on IFNG. This was probably due to IFNG acting on erythroid progenitors, leading to increased erythroid development and early egress of immature erythroid progenitors and reticulocytes to the circulation. The observed reticulocytosis during infection seems to be subjacent to the increased erythrocyte degradation. It is not fully understood why these prematurely released cells have a shorter life span and are removed from circulation. Therefore, further studies are necessary to understand the mechanisms responsible for reduced erythrocyte life span during mycobacterial infection.

In summary, the current study highlights the complexity of the mechanisms behind mycobacteria-induced anemia, suggesting that it is a consequence of the combination of host nutritional immunity to infection, alterations in the kinetics of erythrocyte formation, the triggering of extramedullary erythropoiesis, and increased erythrophagocytosis. The host nutritional immunity involves iron redistribution with a decrease of iron storage in BM. Yet, the cause of anemia is not a block in erythropoiesis. Erythrocytes are still produced, both in the BM and in the spleen, but they are microcytic and have reduced CD47 expression. These changes reduce the half-life of erythrocytes, which are increasingly removed by macrophages, mostly in the liver.

In humans, mycobacterial infections frequently cause anemia, the etiology of which is probably multifactorial (6). The different etiologies of anemia may be related with different presentations of the disease. Disseminated TB, which is relatively rare in humans, shares a lot of similarities with our mouse model of disseminated *M. avium* infection, such as hepatomegaly, splenomegaly, anemia, and colonization of the BM, spleen, and liver (50). In this setting, we found that emergency erythropoiesis occurred in an IFNG-dependent manner. Although the host increased RBC production, anemia established because of decreased erythrocyte life span and increased erythrocyte degradation, suggesting that features of hemolytic anemia account for the establishment of anemia in disseminated mycobacterial infections. The occurrence of hemolytic anemia in TB patients has been occasionally reported, especially during disseminated TB (51–53). More cases may have been overlooked because relevant hematological parameters needed to discriminate between different types of anemia are not usually included in routine assessments.

The prevalence of atypical mycobacterial infection is increasing, and these infections are usually longer and more difficult to treat than TB because of the limited availability of effective antibiotics and also the toxicity of the prolonged antibiotic treatment (2, 54). It is important to emphasize that the work presented in this article corresponds to a systemic infection, and the bacterial loads observed are higher than those usually reported in the clinic. However, we believe the data obtained in this study are highly relevant for the latter stages of infection with atypical mycobacteria, namely when the infection becomes disseminated.

Our findings indicate that a better prevention or treatment of mycobacterial infection-associated anemia should be targeted at increasing the life span of erythrocytes rather than supplementing the host with iron, which has the well-acknowledged risk of causing recrudescence of infection. Additionally, avoiding increased erythrophagocytosis would probably contribute to a better control of mycobacterial infection by preventing heme-associated toxicity.

Acknowledgments

We thank the valuable collaboration of the following i3S Scientific Platforms: the Cell Culture and Genotyping Core Facility, Histology and Electron Microscopy Service, Animal Facility, and Flow Cytometry Unit. The Histology and Electron Microscopy Service is a member of the national infrastructure the Portuguese Platform of Bioimaging (PPBI-POCI-01-0145-FEDER-022122). We further thank Ana Rita Malheiro for help in TEM analysis. We also thank the CoreLab, Centro Hospitalar do Porto, and especially Dr. Graça Henriques for the determination of blood hematological and serum iron parameters. We thank Prof. Michael Jordan, from the Cincinnati Children's Hospital Research Foundation, for providing the initial breeding pairs of MIIG mice and for valuable comments and suggestions for the improvement of this manuscript. We thank Graça Porto and Margarida Lima, from Centro Hospitalar do Porto and the Instituto de Ciências Biomédicas de Abel Salazar, Universidade do Porto, for the critical reading of the manuscript.

Disclosures

The authors have no financial conflicts of interest.

References

1. World Health Organization. 2017. *Global Tuberculosis Report 2017.* World Health Organization, Geneva, Switzerland
2. Adjemian, J., K. N. Olivier, A. E. Seitz, S. M. Holland, and D. R. Prevots. 2012. Prevalence of nontuberculous mycobacterial lung disease in U.S. medicare beneficiaries. *Am. J. Respir. Crit. Care Med.* 185: 881–886.
3. Brode, S. K., C. L. Daley, and T. K. Marras. 2014. The epidemiologic relationship between tuberculosis and non-tuberculous mycobacterial disease: a systematic review. *Int. J. Tuberc. Lung Dis.* 18: 1370–1377.
4. Bastos, H. N., N. S. Osório, A. G. Castro, A. Ramos, T. Carvalho, L. Meira, D. Araújo, L. Almeida, R. Boaventura, P. Fragata, et al. 2016. A prediction rule to stratify mortality risk of patients with pulmonary tuberculosis. *PLoS One* 11: e0162797.
5. Isanaka, S., F. Mugusi, W. Urassa, W. C. Willett, R. J. Bosch, E. Villamor, D. Spiegelman, C. Duggan, and W. W. Fawzi. 2012. Iron deficiency and anemia predict mortality in patients with tuberculosis. *J. Nutr.* 142: 350–357.
6. Minchella, P. A., S. Donkor, O. Owolabi, J. S. Sutherland, and J. M. McDermid. 2015. Complex anemia in tuberculosis: the need to consider causes and timing when designing interventions. *Clin. Infect. Dis.* 60: 764–772.
7. Gil-Santana, L., L. A. B. Cruz, M. B. Arriaga, P. F. C. Miranda, K. F. Fukutani, P. S. Silveira-Mattos, E. C. Silva, M. G. Oliveira, E. D. D. Mesquita, A. Rauwerdink, et al. 2019. Tuberculosis-associated anemia is linked to a distinct inflammatory profile that persists after initiation of antitubercular therapy. *Sci. Rep.* 9: 1381.
8. Rodrigues, P. N., S. S. Gomes, J. V. Neves, S. Gomes-Pereira, M. Correia-Neves, C. Nunes-Alves, J. Stolte, M. Sanchez, R. Appelberg, M. U. Muckenthaler, and M. S. Gomes. 2011. Mycobacteria-induced anaemia revisited: a molecular approach reveals the involvement of NRAMP1 and lipocalin-2, but not of hepcidin. *Immunobiology* 216: 1127–1134.
9. Silva-Gomes, S., S. Vale-Costa, R. Appelberg, and M. S. Gomes. 2013. Iron in intracellular infection: to provide or to deprive? *Front. Cell. Infect. Microbiol.* 3: 96.
10. Moniz, T., A. Nunes, A. M. Silva, C. Queirós, G. Ivanova, M. S. Gomes, and M. Rangel. 2013. Rhodamine labeling of 3-hydroxy-4-pyridinone iron chelators is an important contribution to target *Mycobacterium avium* infection. *J. Inorg. Biochem.* 121: 156–166.
11. Gomes-Pereira, S., P. N. Rodrigues, R. Appelberg, and M. S. Gomes. 2008. Increased susceptibility to *Mycobacterium avium* in hemochromatosis protein HFE-deficient mice. *Infect. Immun.* 76: 4713–4719.
12. Gomes, A. C., A. C. Moreira, G. Mesquita, and M. S. Gomes. 2018. Modulation of iron metabolism in response to infection: twists for all tastes. *Pharmaceuticals (Basel)* 11: 84–101.
13. Weiss, G., T. Ganz, and L. T. Goodnough. 2019. Anemia of inflammation. *Blood* 133: 40–50.
14. Silva-Gomes, S., C. Bouton, T. Silva, P. Santambrogio, P. Rodrigues, R. Appelberg, and M. S. Gomes. 2013. *Mycobacterium avium* infection induces H-ferritin expression in mouse primary macrophages by activating toll-like receptor 2. *PLoS One* 8: e82874.
15. Silva-Gomes, S., R. Appelberg, R. Larsen, M. P. Soares, and M. S. Gomes. 2013. Heme catabolism by heme oxygenase-1 confers host resistance to *Mycobacterium* infection. *Infect. Immun.* 81: 2536–2545.
16. Flórido, M., A. S. Gonçalves, R. A. Silva, S. Ehlers, A. M. Cooper, and R. Appelberg. 1999. Resistance of virulent *Mycobacterium avium* to gamma interferon-mediated antimicrobial activity suggests additional signals for induction of mycobacteriostasis. *Infect. Immun.* 67: 3610–3618.
17. Baldridge, M. T., K. Y. King, N. C. Boles, D. C. Weksberg, and M. A. Goodell. 2010. Quiescent haematopoietic stem cells are activated by IFN-γ in response to chronic infection. *Nature* 465: 793–797.
18. Matatall, K. A., M. Jeong, S. Chen, D. Sun, F. Chen, Q. Mo, M. Kimmel, and K. Y. King. 2016. Chronic infection depletes hematopoietic stem cells through stress-induced terminal differentiation. *Cell Rep.* 17: 2584–2595.
19. Dzierzak, E., and S. Philipsen. 2013. Erythropoiesis: development and differentiation. *Cold Spring Harb. Perspect. Med.* 3: a011601.
20. Inra, C. N., B. O. Zhou, M. Acar, M. M. Murphy, J. Richardson, Z. Zhao, and S. J. Morrison. 2015. A perisinusoidal niche for extramedullary haematopoiesis in the spleen. *Nature* 527: 466–471.
21. Kapur, R., R. Cooper, L. Zhang, and D. A. Williams. 2001. Cross-talk between alpha(4)beta(1)/alpha(5)beta(1) and c-Kit results in opposing effect on growth and survival of hematopoietic cells via the activation of focal adhesion kinase, mitogen-activated protein kinase, and Akt signaling pathways. *Blood* 97: 1975–1981.
22. von Lindern, M., U. Schmidt, and H. Beug. 2004. Control of erythropoiesis by erythropoietin and stem cell factor: a novel role for Bruton's tyrosine kinase. *Cell Cycle* 3: 876–879.
23. Chow, A., M. Huggins, J. Ahmed, D. Hashimoto, D. Lucas, Y. Kunisaki, S. Pinho, M. Leboeuf, C. Noizat, N. van Rooijen, et al. 2013. $CD169^{+}$ macrophages provide a niche promoting erythropoiesis under homeostasis and stress. *Nat. Med.* 19: 429–436.
24. Gomes, A. C., and M. S. Gomes. 2016. Hematopoietic niches, erythropoiesis and anemia of chronic infection. *Exp. Hematol.* 44: 85–91.
25. Theurl, I., I. Hilgendorf, M. Nairz, P. Tymoszuk, D. Haschka, M. Asshoff, S. He, L. M. Gerhardt, T. A. Holderried, M. Seifert, et al. 2016. On-demand erythrocyte disposal and iron recycling requires transient macrophages in the liver. *Nat. Med.* 22: 945–951.
26. Lykens, J. E., C. E. Terrell, E. E. Zoller, S. Divanovic, A. Trompette, C. L. Karp, J. Aliberti, M. J. Flick, and M. B. Jordan. 2010. Mice with a selective impairment of IFN-gamma signaling in macrophage lineage cells demonstrate the critical role of IFN-gamma-activated macrophages for the control of protozoan parasitic infections in vivo. *J. Immunol.* 184: 877–885.
27. Appelberg, R., A. G. Castro, S. Gomes, J. Pedrosa, and M. T. Silva. 1995. Susceptibility of beige mice to *Mycobacterium avium*: role of neutrophils. *Infect. Immun.* 63: 3381–3387.
28. Chow, A., D. Lucas, A. Hidalgo, S. Méndez-Ferrer, D. Hashimoto, C. Scheiermann, M. Battista, M. Leboeuf, C. Prophete, N. van Rooijen, et al. 2011. Bone marrow CD169+ macrophages promote the retention of hematopoietic stem and progenitor cells in the mesenchymal stem cell niche. *J. Exp. Med.* 208: 261–271.
29. Ueda, Y., K. Yang, S. J. Foster, M. Kondo, and G. Kelsoe. 2004. Inflammation controls B lymphopoiesis by regulating chemokine CXCL12 expression. *J. Exp. Med.* 199: 47–58.
30. Ueda, Y., M. Kondo, and G. Kelsoe. 2005. Inflammation and the reciprocal production of granulocytes and lymphocytes in bone marrow. *J. Exp. Med.* 201: 1771–1780.
31. Lousada, S., M. Flórido, and R. Appelberg. 2006. Regulation of granuloma fibrosis by nitric oxide during *Mycobacterium avium* experimental infection. *Int. J. Exp. Pathol.* 87: 307–315.
32. Zoller, E. E., J. E. Lykens, C. E. Terrell, J. Aliberti, A. H. Filipovich, P. M. Henson, and M. B. Jordan. 2011. Hemophagocytosis causes a consumptive anemia of inflammation. *J. Exp. Med.* 208: 1203–1214.
33. Ganz, T., and E. Nemeth. 2012. Iron metabolism: interactions with normal and disordered erythropoiesis. *Cold Spring Harb. Perspect. Med.* 2: a011668.
34. Nai, A., M. R. Lidonnici, M. Rausa, G. Mandelli, A. Pagani, L. Silvestri, G. Ferrari, and C. Camaschella. 2015. The second transferrin receptor regulates red blood cell production in mice. *Blood* 125: 1170–1179.
35. Zhao, B., Y. Mei, J. Yang, and P. Ji. 2016. Erythropoietin-regulated oxidative stress negatively affects enucleation during terminal erythropoiesis. *Exp. Hematol.* 44: 975–981.
36. Kimura, H., C. A. Finch, and J. W. Adamson. 1986. Hematopoiesis in the rat: quantitation of hematopoietic progenitors and the response to iron deficiency anemia. *J. Cell. Physiol.* 126: 298–306.
37. Barclay, A. N., and T. K. Van den Berg. 2014. The interaction between signal regulatory protein alpha (SIRPα) and CD47: structure, function, and therapeutic target. *Annu. Rev. Immunol.* 32: 25–50.

38. Jaiswal, S., C. H. Jamieson, W. W. Pang, C. Y. Park, M. P. Chao, R. Majeti, D. Traver, N. van Rooijen, and I. L. Weissman. 2009. CD47 is upregulated on circulating hematopoietic stem cells and leukemia cells to avoid phagocytosis. *Cell* 138: 271–285.
39. Van, V. Q., M. Raymond, N. Baba, M. Rubio, K. Wakahara, S. A. Susin, and M. Sarfati. 2012. CD47(high) expression on CD4 effectors identifies functional long-lived memory T cell progenitors. *J. Immunol.* 188: 4249–4255.
40. Kuriyama, T., K. Takenaka, K. Kohno, T. Yamauchi, S. Daitoku, G. Yoshimoto, Y. Kikushige, J. Kishimoto, Y. Abe, N. Harada, et al. 2012. Engulfment of hematopoietic stem cells caused by down-regulation of CD47 is critical in the pathogenesis of hemophagocytic lymphohistiocytosis. *Blood* 120: 4058–4067.
41. Muckenthaler, M. U., S. Rivella, M. W. Hentze, and B. Galy. 2017. A red carpet for iron metabolism. *Cell* 168: 344–361.
42. Haldar, M., M. Kohyama, A. Y. So, W. Kc, X. Wu, C. G. Briseño, A. T. Satpathy, N. M. Kretzer, H. Arase, N. S. Rajasekaran, et al. 2014. Heme-mediated SPI-C induction promotes monocyte differentiation into iron-recycling macrophages. *Cell* 156: 1223–1234.
43. McDonald, E. M., M. C. Pilonieta, H. J. Nick, and C. S. Detweiler. 2015. Bacterial stimulation of toll-like receptor 4 drives macrophages to hemophagocytose. *Infect. Immun.* 84: 47–55.
44. Fisman, D. N. 2000. Hemophagocytic syndromes and infection. *Emerg. Infect. Dis.* 6: 601–608.
45. Ramos-Casals, M., P. Brito-Zerón, A. López-Guillermo, M. A. Khamashta, and X. Bosch. 2014. Adult haemophagocytic syndrome. *Lancet* 383: 1503–1516.
46. Schulert, G. S., and A. A. Grom. 2015. Pathogenesis of macrophage activation syndrome and potential for cytokine- directed therapies. *Annu. Rev. Med.* 66: 145–159.
47. Sato, K., N. Misawa, C. Nie, Y. Satou, D. Iwakiri, M. Matsuoka, R. Takahashi, K. Kuzushima, M. Ito, K. Takada, and Y. Koyanagi. 2011. A novel animal model of Epstein-Barr virus-associated hemophagocytic lymphohistiocytosis in humanized mice. *Blood* 117: 5663–5673.
48. Milner, J. D., T. Orekov, J. M. Ward, L. Cheng, F. Torres-Velez, I. Junttila, G. Sun, M. Buller, S. C. Morris, F. D. Finkelman, and W. E. Paul. 2010. Sustained IL-4 exposure leads to a novel pathway for hemophagocytosis, inflammation, and tissue macrophage accumulation. *Blood* 116: 2476–2483.
49. Cnops, J., C. De Trez, B. Stijlemans, J. Keirsse, F. Kauffmann, M. Barkhuizen, R. Keeton, L. Boon, F. Brombacher, and S. Magez. 2015. NK-, NKT- and CD8-derived IFNγ drives myeloid cell activation and erythrophagocytosis, resulting in trypanosomosis-associated acute anemia. *PLoS Pathog.* 11: e1004964.
50. Mert, A., F. Arslan, T. Kuyucu, E. N. Koç, M. Ylmaz, D. Turan, S. Altn, F. Pehlivanoglu, G. Sengoz, D. Yldz, et al. 2017. Miliary tuberculosis: epidemiologicaland clinical analysis of large-case series from moderate to low tuberculosis endemic country. *Medicine (Baltimore)* 96: e5875.
51. Blanche, P., A. Rigolet, P. P. Massault, D. Bouscary, F. Dreyfus, and D. Sicard. 2000. Autoimmune haemolytic anaemia revealing miliary tuberculosis. *J. Infect.* 40: 292.
52. Kuo, P. H., P. C. Yang, S. S. Kuo, and K. T. Luh. 2001. Severe immune hemolytic anemia in disseminated tuberculosis with response to antituberculosis therapy. *Chest* 119: 1961–1963.
53. Rathish, D., and S. Siribaddana. 2018. Tuberculosis induced autoimmune haemolytic anaemia: a systematic review to find out common clinical presentations, investigation findings and the treatment options. *Allergy Asthma Clin. Immunol.* 14: 11.
54. Antunes, A., F. Viveiros, A. Carvalho, and R. Duarte. 2012. Micobactérioses Não-tuberculosas – das manifestações clínicas ao tratamento. *Arq. Med.* 26: 25–30.